COMMUNICATION

Check for updates

Solvent-induced structural transformation in a one-dimensional coordination polymer†

Kangwoo Jin,[a] Nohyoon Park,[a] Yongdeok Ahn,[a] Daeha Seo,[a] Dohyun Moon, [ID] *[b] Jooyoung Sung*[a] and Jinhee Park [ID] *[a]

We have rationally designed a one-dimensional coordination polymer (1D CP), termed 1D-DGIST-18, that exhibits intrinsic structural flexibility. This 1D CP enables its expansion into a three-dimensional network through supramolecular interactions involving coordinated solvents and/or ligands. The strategic selection of solvents for solvent exchange, prior to drying, significantly influences the structures of 1D-DGIST-18 by removing certain coordinating solvents and modulating π–π stacking. Consequently, a hierarchical porosity emerges, ranging from micro- to meso- to macroporous structures, which is attributed to its inherent structural dynamics. Additionally, the formation of excimers endows 1D-DGIST-18, when immersed in acetone, with 'turn-on' fluorescence, as evidenced by fluorescence decay profiles. These structural transitions within 1D-DGIST-18 are further elucidated using single-crystal X-ray diffractometry. The insights from this study provide a foundation for the design of materials with structural dynamics and tunable properties.

[a]Department of Physics and Chemistry, Daegu-Gyeongbuk Institute of Science and Technology, Daegu 42988, the Republic of Korea. E-mail: jooyoung@dgist.ac.kr, jinhee@dgist.ac.kr

[b]Beamline Department, Pohang Accelerator Laboratory, Pohang 37673, the Republic of Korea. E-mail: dmoon@postech.ac.kr

Jinhee Park earned her PhD in chemistry from Texas A&M University in 2013, under the esteemed supervision of Prof. Hong-Cai "Joe" Zhou. After working as a senior researcher in the Korea Electrotechnology Research Institute, she joined the faculty of Daegu Gyeongbuk Institute of Science and Technology (DGIST) in 2016. Her research centers on pioneering porous materials tailored for environmental and energy solutions.

Jinhee Park

Lowering the dimensionality of metal–ligand networks in coordination polymers (CPs), also known as metal–organic frameworks (MOFs), improves their structural flexibility and dynamic behavior.[1] In particular, one-dimensional (1D) CPs have been in the spotlight for the last decade because of their interesting architectures and properties (*e.g.*, magnetism, electrical conductivity, and optical changes).[2–4] However, 1D CPs are typically nonporous owing to the absence of rigid spacers between their 1D linear, helical, and zigzag chains; solvent removal causes the adjacent chains to draw closer, eliminating the spaces between them. Although there have been some rare cases of 1D CPs exhibiting microporosity arising from their structural rigidities, they function as rigid three-dimensional (3D) networks, with negligible dynamic behavior and a corresponding lack of transformative porosities.[5–8] Therefore, strong yet flexible supramolecular interactions such as π–π interactions, hydrogen bonding, and van der Waals forces have emerged as important factors in the design of 1D CPs.

The 1,8-naphthalimide unit, which is π-electron-deficient owing to its electron-withdrawing imide group, can promote directional π–π stacking.[9,10] Additionally, the 1,8-naphthalimide moiety can easily rotate on a single N–C bond, and their π–π stacks slip upon changes in the surrounding environment; these dynamics have been documented in some crystal structures.[11,12] However, they have rarely been translated into dynamic porosities because most examples exhibited dense π-stacking, resulting in nonporous structures.[13,14] In this study, we developed a 1,8-naphthalimide-based 1D CP that demonstrates unprecedented hierarchical porosity influenced by solvent treatment. Pronounced face-to-face π–π interactions occurred, which led to the formation of J-type and H-type aggregates.[15–17] Intriguingly, specific solvent treatment, such as with acetone, induced excimer formation, resulting in red-shifted, brilliant blue fluorescence, highlighting the structural flexibility of the CP.

We prepared Zn-based 1D and 3D CPs to elucidate the significance of combining flexible scaffolds with 1,8-naphthalimide units. $Zn(OAc)_2 \cdot 2H_2O$ and H_2L (L^{2-} = 5-(1,8-naphthalimido)-isophthalate) individually dissolved in dimethyl sulfoxide (DMSO) were mixed and allowed to react under ambient conditions for 1 d, which afforded colorless single crystals (1D-DGIST-18). The formula of 1D-DGIST-18 was identified by single-crystal X-ray diffractometry (SCXRD) as $[ZnL(DMSO)_2]$, which crystallized with a monoclinic $P2_1/n$ space group. In this structure, the naphthyl moieties of L^{2-} were arranged along the zigzag chains (Fig. 1a, inset). The ditopic L^{2-} linkers were connected to tetrahedrally coordinated mononuclear Zn^{2+} ions in a monodentate manner (η^1 mode) along the c-axis (Fig. 1a). The remaining sites for the Zn^{2+} ions were occupied by two disordered DMSO molecules. The O–Zn–O angle between the two linkers and Zn^{2+} was approximately 116.8°. The dangling naphthyl rings of L^{2-} faced the adjacent naphthyl ring from other chains at a perpendicular planar distance of 3.7 Å, indicating that two-dimensional (2D) sheets were formed through π–π interactions *via* head-to-tail superimposition.[18] In the view along the c-axis, the 2D sheet exhibited an uneven texture attributed to the tilted naphthyl rings and their alternating π

stacking (Fig. 1b). The interlayer distance from the upper Zn^{2+} ion to the lower Zn^{2+} ion was 5.8 Å. Each layer weakly interacted *via* C–H⋯O hydrogen bonds between DMSO molecules on the upper and lower layers; the distance between O (O8A) in the upper DMSO and H (H24A) in the lower DMSO was 2.87 Å (Fig. 1b). The π stack formation of the ligand H_2L was monitored *via in situ* ^{1}H-NMR studies in DMSO-d_6. All peaks corresponding to the 1,8-naphthalimide unit shifted and broadened with increasing reaction time, indicating the π-stacking of aromatic moieties.[19,20] The ^{1}H-NMR data of H_2L in DMSO-d_6 in the absence of $Zn(OAc)_2 \cdot 2H_2O$ exhibited no chemical shift for 1 d, implying that the formation of Zn–O coordination triggered π–π interactions (Fig. 1c).[20]

Meanwhile, a mixture of $Zn(OAc)_2 \cdot 2H_2O$ and H_2L dispersed in *N,N*-dimethylformamide (DMF) at 120 °C yielded a 3D CP $[ZnL(DMF)_{1.5}]$, hereinafter referred to as 3D-DGIST-18, which featured a 3D scaffold derived from binuclear Zn^{2+} clusters. 3D-DGIST-18 (*Cc* space group) was assembled through diverse Zn^{2+}–COO^- binding modes (Fig. 1d). The Zn^{2+} clusters were composed of four-coordinated and six-coordinated Zn^{2+} ions bridged by two carboxylates from two L^{2-} linkers (μ_2-η^1:η^1 mode) and an oxygen atom (μ_2-η^2 mode) of one L^{2-} linkers.
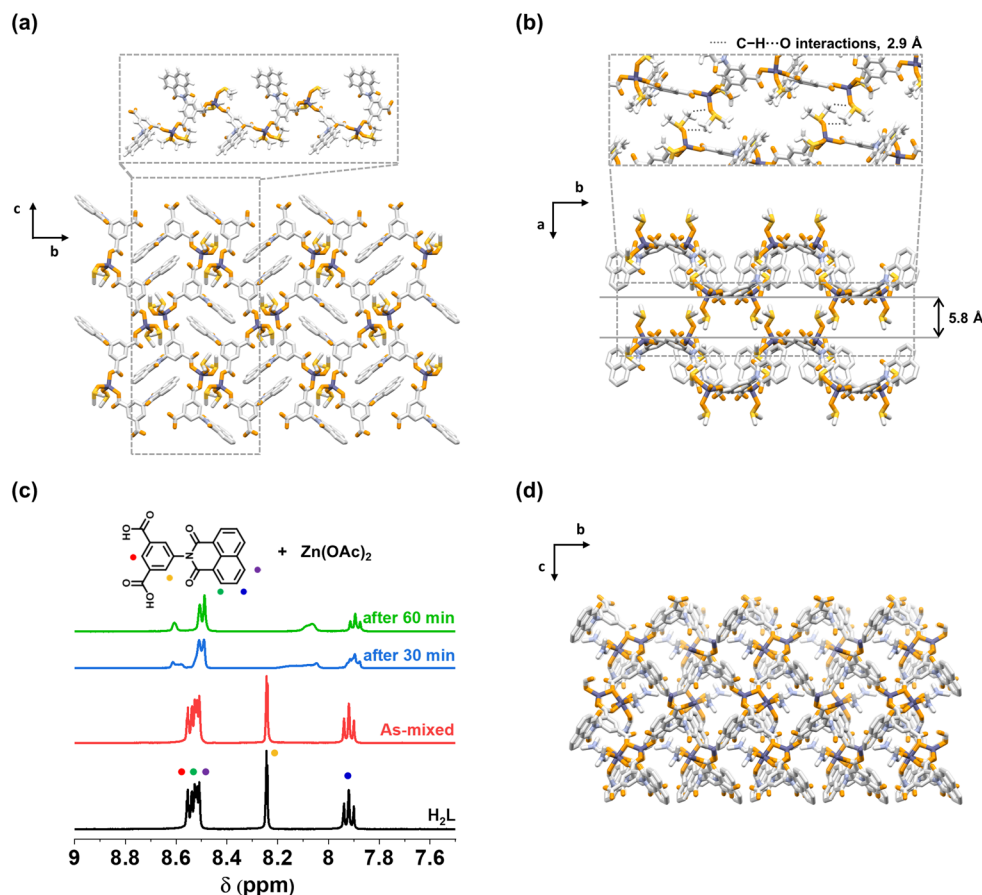

Fig. 1 (a) The 2D supramolecular layer structure of 1D-DGIST-18, assembled *via* π–π interactions in the 1D zigzag chain. (b) Cross-sectional view of 1D-DGIST-18; (inset) C–H⋯O hydrogen bonds between DMSO in neighboring layers. (c) *In situ* NMR spectra monitoring the rapid formation of π–π interactions in 1D-DGIST-18 in DMSO-d_6. (d) Representation of the crystal structure of 3D-DGIST-18. Blue, Zn; orange, O; yellow, S; gray, C; pale blue, N; and white, H. Hydrogen atoms are omitted for clarity.

To confirm the permanent porosity of the two CPs, solvent exchange followed by activation procedures was conducted. The application of direct vacuum to 1D-DGIST-18 necessitated high temperatures to remove DMSO. We therefore sought for an appropriate solvent with a low boiling point and moderate coordination strength to substitute the strongly coordinated DMSO on 1D-DGIST-18 while having little impact on the overall structure of 1D-DGIST-18. Powder X-ray diffraction (PXRD) patterns of 1D-DGIST-18 immersed in various solvents showed that it rapidly changed to different phases in polar and strongly coordinating solvents, such as ethanol, methanol, isopropyl alcohol, and tetrahydrofuran (Fig. S3†). However, in weakly coordinating or noncoordinating solvents such as hexane, cyclohexane, toluene, chloroform, dichloromethane, acetone, and diethyl ether, the crystal structures of 1D-DGIST-18 were preserved or underwent only minor phase transformations (Fig. S3†). Based on these observations, acetone was selected owing to its weak coordination properties, offering potential for the gentle removal of DMSO from 1D-DGIST-18.

Fortunately, we obtained a single-crystal structure after immersing 1D-DGIST-18 in acetone under ambient conditions for 1 d; hereinafter, the structure is referred to as 1D-DGIST-18′. Water molecules present in the solvent or atmosphere preferentially displaced the DMSO molecules, which dissociated the C–H⋯O hydrogen bonds between the DMSO molecules, resulting in the interlayer distance based on Zn decreasing from 5.8 Å to 1.2 Å (Fig. 2a). This dissociation significantly altered the interlayer interactions, correspondingly implying the structural flexibility and dynamic behavior of 1D-DGIST-18. In the unit cell of 1D-DGIST-18′, the following occurred: the length of the a-axis, along which the 2D layers were stacked, noticeably decreased from 12.558(3) Å to 8.5630 (17) Å. The dihedral angle of the naphthalimide moiety increased from 70.2° to 86.6° and the O–Zn–O angles between the two linkers and the Zn node decreased from 116.8° to 113.8°. These notable alterations in the structure highlight the exceptional flexibility inherent to 1D-DGIST-18. The transient state, 1D-DGIST-18′, is characterized by increased disorders and decreased crystallinity during acetone exchange, contributing to the increased R factor in the crystallographic analysis.

During the acetone exchange process, the amount of DMSO remaining on 1D-DGIST-18 was monitored by ^{1}H-NMR. For the NMR monitoring, small amounts of 1D-DGIST-18 were subjected to decomposition using 0.1 M NaOH in D_2O, following which their spectra were obtained (Fig. 2b). The peak at approximately 2.7 ppm represents the 6H of DMSO. However,
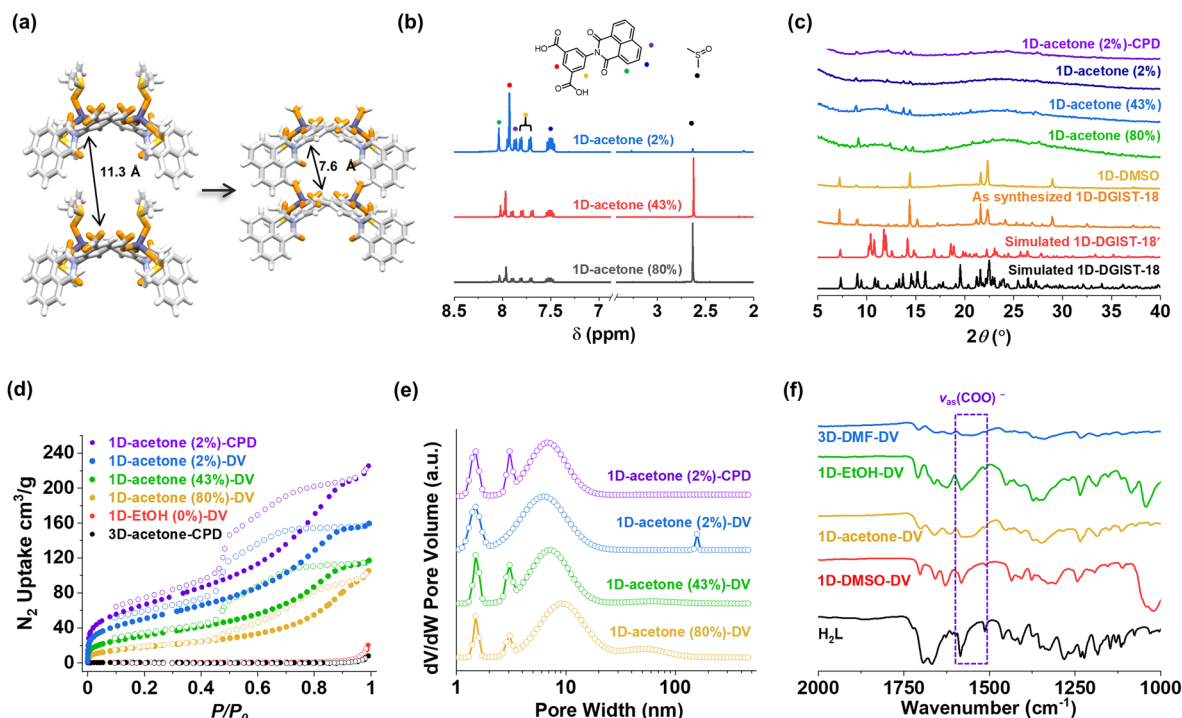

Fig. 2 (a) Cap-and-stick representation of (left) 1D-DGIST-18 and (right) 1D-DGIST-18′ and changes in Zn to O of monodentate COO⁻ distance between adjacent layers. Color codes: blue, Zn; orange, O; yellow, S; gray, C; pale blue, N; and white, H. (b) ^{1}H-NMR spectra of the 1D-DGIST-18 samples treated with acetone after deprotonation using 0.1 M NaOH in D_2O. (c) PXRD patterns for simulated 1D-DGIST-18, simulated 1D-DGIST-18′, as-synthesized 1D-DGIST-18, 1D-DMSO, 1D-acetone (2–80%), and 1D-acetone (2%)-CPD. (d) N_2 adsorption–desorption isotherms for 1D-DGIST-18 after various solvent treatments and 3D-DGIST-18 after acetone treatment, recorded at 77 K. (e) NLDFT pore-size distribution of 1D-acetone (2–80%)-DV and 1D-acetone (2%)-CPD derived from the N_2 adsorption isotherms. (f) IR spectra of H_2L, 1D-DGIST-18, and 3D-DGIST-18 after treatment with various solvents followed by drying.

due to its strong coordination, it was difficult to remove all the coordinated DMSO. Accordingly, we employed Soxhlet extraction to further eliminate DMSO. Three 1D-DGIST-18 samples with different amounts of residual DMSO (2%, 43%, and 80%) were prepared to compare their porosities.

Hereinafter, we will refer to samples as "A–B (C%)–D", where 'A' is the dimension of the MOF (1D or 3D), 'B' is the solvent used for treatment, '(C%)' is the residual DMSO in 1D-DGIST-18, and 'D' is the drying method (CO_2 supercritical point drying (CPD) or direct vacuum (DV)). The omission of 'D' implies a wet sample. The decreased intensities of the PXRD patterns for 1D-acetone shows that with increasing exclusion of the DMSO molecules by water or acetone, the 1D-DGIST-18 crystal lost its ordered structure (Fig. 2c). Eventually, the PXRD patterns of 1D-acetone-DV almost disappeared (Fig. S4†). Meanwhile, with decreasing DMSO, the Brunauer–Emmett–Teller (BET) surface areas of 1D-acetone (2–80%)-DV samples gradually increased, with values of 61, 115, and 185 m^2 g^{-1} for 80%, 43%, and 2% remnant DMSO, respectively (Fig. 2d). Lastly, the BET surface area increased with the use of CPD for drying, with 1D-acetone (2%)-CPD exhibiting an area of 243 m^2 g^{-1}. This result implies that CO_2 CPD, due to its low surface tension, enables the gentle removal of acetone while effectively preserving the porous structures the material.[21] N_2 adsorption–desorption isotherms of all 1D-acetone (2–80%) samples exhibited a combination of type I, II, and IV isotherms and exceptionally wide hysteresis.[22] Pore-size distribution curves were calculated using the non-local density functional theory (NLDFT) method; the pore sizes varied from micro- to macropores depending on the solvent and drying method (Fig. 2e). Supplementary CO_2 and H_2 adsorption–desorption isotherms for 1D-acetone (2%)-CPD are presented respectively in Fig. S7 and S8.† The pore size distribution, derived from the CO_2 adsorption isotherm, characterizes the presence of small micropores. Additionally, the significant hysteresis observed in the H_2 adsorption–desorption isotherms confirms the flexible nature of activated 1D-DGIST-18.[23] However, 1D-DGIST-18 samples soaked in polar and strongly coordinating solvents, such as 1D-ethanol (0%)-CPD and 1D-methanol (0%)-CPD, transformed to nonporous structures with BET surface areas of approximately 3 m^2 g^{-1} (Fig. 2d and S10†). Furthermore, SEM images of 1D-ethanol (0%)-CPD and 1D-methanol (0%)-CPD showed significant cracks on their surfaces, whereas the 1D-acetone (2%)-CPD sample displayed a relatively flat surface (Fig. S12–S14†).

The diverse structural transformation of 1D-DGIST-18 was attributed to the flexible Zn^{2+} nodes. The monodentate carboxylate (η^1 mode) of L^{2-} in 1D-DGIST-18 further bound to Zn^{2+} upon the substitution of coordinated solvents. IR spectra indicated the changes in the stretching vibration mode of the carboxylate of L^{2-} (Fig. 2f). The IR spectrum of pristine 1D-DGIST-18 initially displayed a peak at 1581 cm^{-1}, while that of 1D-acetone-DV displayed a broad peak in the range of 1550–1580 cm^{-1}, possibly owing to the coexistence of the monodentate (η^1) mode with the bridging (μ_2-η^1:η^1) and monoatomic bridging (μ_2-η^2) binding modes.[24] Similarly, the

IR spectrum of the 1D-EtOH (0%)-DV sample exhibited slight broadening. The 3D-DMF-DV samples, which has diverse Zn–COO^- binding modes including the monodentate, bridging, and monoatomic bridging modes, showed a broad peak at approximately 1550–1580 cm^{-1}. Additionally, the monomeric Zn^{2+} ion on the 1D backbone has a flexible coordination environment;[5,25] the changes in coordination geometry of the four-coordinated Zn^{2+} ion upon coordinated-solvent removal can distort the 1D chains. Consequently, the 1D-acetone-DV samples exhibited various defects, resulting in the formation of hierarchically porous structures.

The single crystal of 1D-DGIST-18′ exhibited a microporous structure with a network-accessible geometric volume of 0.280 cm^3 g^{-1}, as determined by the Pore Analyser in Mercury software. However, this structure gradually transformed into a hierarchically porous structure following Soxhlet extraction with acetone and CPD. Meanwhile, despite the single-crystal structure of 3D-DGIST-18 displaying a comparable volume of 0.273 cm^3 g^{-1}, it was not porous (Fig. 2d). As the PXRD measurements indicated a decline in crystallinity of 3D-DGIST-18 in the presence of acetone, we conducted DMF washing and CPD to preserve its structure. However, the PXRD patterns confirmed a collapsed structure after solvent removal (Fig. S6†). A subsequent N_2 sorption experiment consistently demonstrated minimal N_2 uptake (Fig. S11†).

Interestingly, we observed "turn-on" fluorescent behavior when 1D-DMSO transitioned to 1D-acetone, underscoring the influence of the solvent-dependent structural changes, particularly in the π-stacks of the ligands (Fig. 3). As shown in Fig. S15,† the absorption spectra of 1D-DMSO and 1D-acetone are nearly identical. However, there is a marked contrast in their fluorescence excitation spectra and accompanying fluorescence emission spectra, as depicted in Fig. 4a and b, respectively. The fluorescence excitation spectrum of 1D-DMSO recorded at 450 nm reveals two distinct peaks at approximately 370 and 390 nm with a negligible Stokes shift between the excitation and fluorescence spectra. In sharp contrast, 1D-acetone lacks the fluorescence excitation band at 390 nm but displays a red-shifted and broad fluorescence emission spectrum. Notably, as shown in the inset of Fig. 4b,
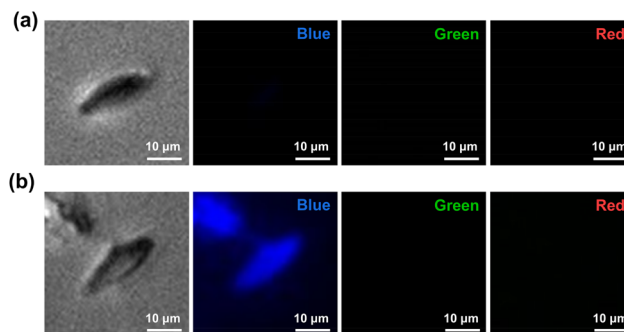

Fig. 3 Bright-field and fluorescence images of (a) 1D-DMSO and (b) 1D-acetone (2%). The excitation and emission specifications for the filter cube sets can be found in Table S3.†
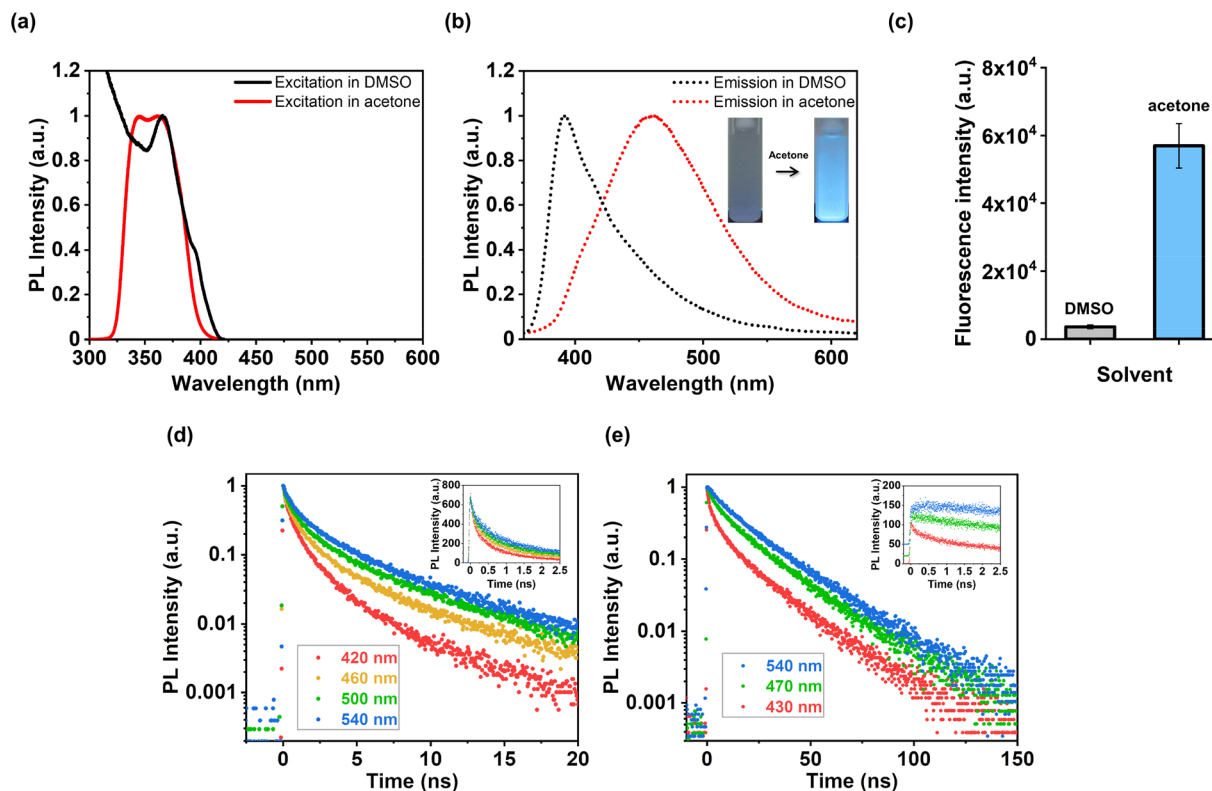
Fig. 4 Fluorescence (a) excitation and (b) emission spectra of 1D-DMSO and 1D-acetone (2%). (c) Average pixel intensities of 1D-DMSO and 1D-acetone (2%) images. Fluorescence decay profiles of (d) 1D-DMSO and (e) 1D-acetone (2%).

1D-acetone (2%) exhibits a brighter blue emission than that of 1D-DMSO. Quantitatively, the average pixel intensity of the image under 435–485 nm light irradiation is estimated to be approximately 16-fold greater for 1D-acetone (2%) than for 1D-DMSO (Fig. 4c). While the disparities observed in fluorescence excitation and emission spectra and fluorescence quantum yields between 1D-DMSO and 1D-acetone strongly imply their structural differences, it remains unclear whether 1D-DMSO and 1D-acetone manifest H- or J-type aggregates or form excimers.

To gain deeper understanding of the structural distinctions and concomitant fluorescence characteristics between 1D-DMSO and 1D-acetone, we conducted time-correlated single photon counting (TCSCP) measurements for both CPs. As depicted in Fig. 4d and e, 1D-DMSO and 1D-acetone showed markedly different fluorescence decay profiles. For 1D-DMSO, the fluorescence kinetics monitored at different wavelengths exhibited multiexponential behavior and were thus fitted with the stretched exponential functions. The fluorescence lifetime values for 1D-DMSO and 1D-acetone (2%) are shown in Table 1. The stretching exponent β_1 is expected to be in the range 0–1, with the deviation from 1 corresponding to the degree of dynamic heterogeneity. A β_1 of approximately 0.65 was obtained for 1D-DMSO, signifying dynamic heterogeneity due to the structural diversity in 1D-DMSO. Importantly, the fluorescence kinetics of 1D-DMSO were com-

Table 1 Fluorescence lifetime values for 1D-DMSO and 1D-acetone (2%)

	λ (nm)	t_1 (ns)	t_2 (ns)	β_1
1D-DMSO	420	0.3 (0.74)	1.8 (0.26)	0.84
	460	0.5 (0.89)	4.7 (0.11)	0.67
	500	0.6 (0.82)	4.9 (0.18)	0.70
	540	0.7 (0.83)	5.5 (0.17)	0.65
1D-acetone (2%)	430	2.0 (0.79)	19.3 (0.21)	0.61
	470	3.5 (0.56)	18.7 (0.44)	0.76
	540	6.2 (0.34)	21.3 (0.66)	0.97

pleted within 25 ns with time constants faster than 1 and 6 ns, which is consistent with the lifetime of naphthalimide.[26] The obtained fluorescence lifetime of less than 6 ns and fluorescence excitation bands at 390 nm with the negligible Stokes shift suggest that the predominant fluorescence species in 1D-DMSO were J-type aggregates.[27,28] However, the short decay component with the small β_1 of approximately 0.65 and relatively low fluorescence quantum yields of 1D-DMSO indicate the presence of efficient nonradiative decay channels in 1D-DMSO and further suggest the coexistence of H-type aggregates.

Interestingly, the fluorescence decay profiles of the 1D-acetone were completed within 150 ns. Previous research has shown that the fluorescence lifetime of 1,8-naphthalimide

excimeric species is long, typically ranging between 8 and 20 ns.[17,29,30] Therefore, the extended decay time observed in acetone can be assigned to excimer formation. Furthermore, the early-time decay profile probed at 430 nm exhibits a decay component of 200 ps, while the profile probed at 540 nm shows a rise component of 200 ps (Fig. 4e, inset). The observed rise and decay dynamics further support the existence of the excimer species.[31] The excimer formation in 1D-acetone (2%) serves as compelling evidence of DGIST-18 undergoing a structural transition during solvent exchange. Excimer states are typically expected to form within a 3–5 Å interplanar distance despite the disorder introduced by acetone, the L^{2-} ligands in 1D-acetone (2%) remained closely positioned, ensuring that the porosity was retained after drying.[30,31] This observation supports our assertion that the material retains its integrity while exhibiting structural flexibility.

In conclusion, this study highlights the unique hierarchical porosity and 'turn-on' fluorescence behavior of the flexible 1D CP, DGIST-18, that were imparted by its structural transformation. The transition of 1D-DGIST-18 from a crystalline phase to an amorphous phase occurred *via* the shedding of coordinated solvents and formation of additional Zn–COO⁻ linkages during solvent exchange and drying processes. An intermediate state, termed 1D-DGIST-18′, was characterized using SCXRD, revealing a significantly reduced interlayer distance compared to that of its pristine structure. Furthermore, variation in the aromatic interactions within the ligand was verified by observing the formation of excimers. Overall, this study presents a pioneering design strategy for the transformation of low-dimensional materials into porous architectures.

Author contributions

K. J. and J. P. conceived the idea and wrote the manuscript. K. J., N. P., Y. A., D. M., and J. S. performed the experiments. All authors contributed to the interpretation of the results and approved the final version of the manuscript.

Conflicts of interest

There are no conflicts to declare.

Acknowledgements

References

1 M. Lippi and M. Cametti, *Coord. Chem. Rev.*, 2021, **430**, 213661.

2 W. L. Leong and J. J. Vittal, *Chem. Rev.*, 2011, **111**, 688–764.

3 F. Ahmed, B. Dutta and M. H. Mir, *Dalton Trans.*, 2021, **50**, 29–38.

4 S. Shang, C. Du, Y. Liu, M. Liu, X. Wang, W. Gao, Y. Zou, J. Dong, Y. Liu and J. Chen, *Nat. Commun.*, 2022, **13**, 7599.

5 A.-L. Cheng, N. Liu, Y.-F. Yue, Y.-W. Jiang, E.-Q. Gao, C.-H. Yan and M.-Y. He, *Chem. Commun.*, 2007, 407–409.

6 J.-H. Deng, J. Luo, Y.-L. Mao, S. Lai, Y.-N. Gong, D.-C. Zhong and T.-B. Lu, *Sci. Adv.*, 2020, **6**, eaax9976.

7 S. Takamizawa, E.-I. Nakata and T. Saito, *Inorg. Chem. Commun.*, 2004, **7**, 125–127.

8 G. K. Kole, A. J. Cairns, M. Eddaoudi and J. J. Vittal, *New J. Chem.*, 2010, **34**, 2392–2395.

9 D. L. Reger, A. Debreczeni, B. Reinecke, V. Rassolov, M. D. Smith and R. F. Semeniuc, *Inorg. Chem.*, 2009, **48**, 8911–8924.

10 S. Banerjee, E. B. Veale, C. M. Phelan, S. A. Murphy, G. M. Tocci, L. J. Gillespie, D. O. Frimannsson, J. M. Kelly and T. Gunnlaugsson, *Chem. Soc. Rev.*, 2013, **42**, 1601–1618.

11 D. L. Reger, A. Debreczeni and M. D. Smith, *Inorg. Chem.*, 2011, **50**, 11754–11764.

12 D. L. Reger, A. Leitner, P. J. Pellechia and M. D. Smith, *Inorg. Chem.*, 2014, **53**, 9932–9945.

13 R. Haldar, R. Matsuda, S. Kitagawa, S. J. George and T. K. Maji, *Angew. Chem., Int. Ed.*, 2014, **53**, 11772–11777.

14 L. Li, L. Guo, D. H. Olson, S. Xian, Z. Zhang, Q. Yang, K. Wu, Y. Yang, Z. Bao, Q. Ren and J. Li, *Science*, 2022, **377**, 335–339.

15 M. Kumar and S. J. George, *Chem. – Eur. J.*, 2011, **17**, 11102–11106.

16 P. Gopikrishna, N. Meher and P. K. Iyer, *ACS Appl. Mater. Interfaces*, 2018, **10**, 12081–12111.

17 C. Felip-León, F. Galindo and J. F. Miravet, *Nanoscale*, 2018, **10**, 17060–17069.

18 J. K. Nath and J. B. Baruah, *CrystEngComm*, 2015, **17**, 8575–8595.

19 X. Cao, L. Meng, Z. Li, Y. Mao, H. Lan, L. Chen, Y. Fan and T. Yi, *Langmuir*, 2014, **30**, 11753–11760.

20 D. Niu, Y. Jiang, L. Ji, G. Ouyang and M. Liu, *Angew. Chem., Int. Ed.*, 2019, **58**, 5946–5950.

21 A. J. Howarth, A. W. Peters, N. A. Vermeulen, T. C. Wang, J. T. Hupp and O. K. Farha, *Chem. Mater.*, 2017, **29**, 26–39.

22 M. Thommes, K. Kaneko, A. V. Neimark, J. P. Olivier, F. Rodriguez-Reinoso, J. Rouquerol and K. S. W. Sing, *Pure Appl.*, 2015, **87**, 1051–1069.

23 X. Zhao, B. Xiao, A. J. Fletcher, K. M. Thomas, D. Bradshaw and M. J. Rosseinsky, *Science*, 2004, **306**, 1012–1015.

24 V. Zeleňák, Z. Vargová and K. Györyová, *Spectrochim. Acta, Part A*, 2007, **66**, 262–272.

25 A. Erxleben, *Coord. Chem. Rev.*, 2003, **246**, 203–228.

26 R. K. Dubey, D. Inan, S. Sengupta, E. J. R. Sudhölter, F. C. Grozema and W. F. Jager, *Chem. Sci.*, 2016, **7**, 3517–3532.

27 M. Kasha, H. R. Rawls and M. Ashraf El-Bayoumi, *Pure Appl. Chem.*, 1965, **11**, 371–392.

28 N. J. Hestand and F. C. Spano, *Chem. Rev.*, 2018, **118**, 7069–7163.

29 T. C. Barros, P. B. Filho, V. G. Toscano and M. J. Politi, *J. Photochem. Photobiol., A*, 1995, **89**, 141–146.

30 R. Ferreira, C. Baleizão, J. M. Muñoz-Molina, M. N. Berberan-Santos and U. Pischel, *J. Phys. Chem. A*, 2011, **115**, 1092–1099.

31 Y. Hong, W. Kim, T. Kim, C. Kaufmann, H. Kim, F. Würthner and D. Kim, *Angew. Chem., Int. Ed.*, 2022, **61**, e202114474.